energies

MDPI

Article

Lattice Boltzmann Simulation of Optimal Biphilic Surface Configuration to Enhance Boiling Heat Transfer

Alexander V. Fedoseev [1,*], Mikhail V. Salnikov [1], Anastasiya E. Ostapchenko [1] and Anton S. Surtaev [1,2]

[1] Institute of Thermophysics SB RAS, Lavrentyev Ave. 1, Novosibirsk 630090, Russia
[2] Physics Department, Novosibirsk State University, Pirogova Str. 2, Novosibirsk 630090, Russia
* Correspondence: fedoseev@itp.nsc.ru

Abstract: To study the processes of boiling on a smooth surface with contrast wettability, a hybrid model was developed based on Lattice Boltzmann method and heat transfer equation. The model makes it possible to describe the phenomena of natural convection, nucleate boiling, and transition to film boiling, and, thus, to study heat transfer and the development of crisis phenomena in a wide range of surface superheats and surface wetting characteristics. To find the optimal configuration of the biphilic surface, at the first stage a numerical simulation was carried out for a single lyophobic zone on a lyophilic surface. The dependences of the bubble departure frequency and the departure diameter of the bubble on the width of the lyophobic zone were obtained, and its optimal size was determined. At the next stage, the boiling process on an extended surface was studied in the presence of several lyophobic zones of a given size with different distances between them. It is shown that in the region of moderate surface superheat, the intensity of heat transfer on biphilic surfaces can be several times (more than 4) higher compared to surfaces with homogeneous wettability. Based on numerical calculations, an optimal configuration of the biphilic surface with the ratios of the lyophobic zones' width of the order of 0.16 and the distance between the lyophobic zones in the range of 0.9–1.3 to the bubble departure diameter was found.

Keywords: pool boiling; heat transfer enhancement; biphilic surface; lattice Boltzmann method

check for updates

Citation: Fedoseev, A.V.; Salnikov, M.V.; Ostapchenko, A.E.; Surtaev, A.S. Lattice Boltzmann Simulation of Optimal Biphilic Surface Configuration to Enhance Boiling Heat Transfer. *Energies* **2022**, *15*, 8204. https://doi.org/10.3390/en15218204

Academic Editor: Marco Marengo

Received: 12 October 2022
Accepted: 1 November 2022
Published: 3 November 2022

Publisher's Note: MDPI stays neutral with regard to jurisdictional claims in published maps and institutional affiliations.

Copyright: © 2022 by the authors. Licensee MDPI, Basel, Switzerland. This article is an open access article distributed under the terms and conditions of the Creative Commons Attribution (CC BY) license (https://creativecommons.org/licenses/by/4.0/).

1. Introduction

To date, issues related to the enhancement of heat transfer during liquid boiling have received great attention from scientists and engineers, which is confirmed by numerous papers and reviews published in the past few years [1–5]. This is due to a wide range of practical applications in which the boiling process plays a key role. One of the most popular and effective methods for the enhancement of the heat transfer and increasing the critical heat flux (CHF) during boiling is the modification of the heat exchange surface. Surface modification can be implemented both by structuring the original surface using, for example, mechanical machining or laser texturing, and by fabrication of micro/nanostructured porous coatings [5]. As a result of heat exchange surface modifications, not only the morphology, but also the wetting characteristics can change. It is known that wetting properties have a significant effect on the heat transfer intensity and the development of crisis phenomena during liquid boiling. For example, the use of superhydrophilic micro- or nanoporous surfaces leads to a significant increase in the CHF value at parameters corresponding to water boiling (up to 2–3 times) [6,7]. In turn, the use of weakly hydrophobic coatings leads to a decrease in the temperature of the onset of nucleate boiling (ONB), to an increase in the nucleation site density and the heat transfer enhancement in the regions of low heat fluxes [8–11]. However, the CHF significantly decreases when using hydrophobic and superhydrophobic coatings [11–13]. In particular, in [10,11] during water boiling on flat and tubular hydrophobic heat exchange surfaces (contact angle $\theta \approx 125^\circ$), heat transfer enhancement was found in the region of low heat fluxes ($q < 100$–150 kW/m^2) compared to

heat transfer on the base hydrophilic surface. Moreover, the use of the developed hydrophobic coatings can significantly reduce the temperature of the onset of water boiling (up to 2–3° K), especially during boiling at subatmospheric pressures [11]. However, the CHF decreases significantly when using hydrophobic and superhydrophobic coatings [11–13]. For example, in an experimental study [12] it was shown that the usage of a superhydrophobic heated surface (contact angle $\theta \approx 165°$), vapor film is almost immediately formed at 1–2° K of superheating, covering the entire surface, thus the heat transfer is reduced just after the onset of boiling.

One of the modern trends in the field of material science in relation to the problems of improvement of pool boiling performance is the fabrication of biphilic surfaces or, in other words, surfaces with contrast wettability. The use of biphilic surfaces, as shown by the analysis of recent papers [14–17], permits simultaneously increasing the heat transfer intensity by reducing the bubbles activation threshold and increasing CHF due to more efficient wetting of dry spots in precrisis modes and modulation of the two-phase flows near the heated wall. In particular, it was shown in experiments [14,15] that the use of biphilic coatings can lead to an increase in the heat transfer coefficient and CHF values up to 5 and 2 times, respectively. At the same time, the task of determination of the biphilic surface configuration for the optimal boiling conditions remains open. These configurations vary for different liquids and boiling regimes including pressure change.

The search for the optimal configuration of a surface with contrast wettability based on experimental studies is a rather laborious task, the complexity of which is primarily determined by the creation of stable coatings with the ability to control the geometric parameters of the structure at various scales, including micro and nanoscales. An additional complication is the requirement for high-precision high-speed measurements to study the evolution of vapor bubbles and a two-phase layer near the surface using a set of modern experimental methods. With the rapid development of computer technology, computational fluid dynamics (CFD) methods have proven to be a good alternative to experiment for studying two-phase flows, including those in which phase transitions occur [18–26]. The classical approach to modeling two-phase flows, including boiling, is reduced to the numerical solution of the Navier–Stokes equations in combination with an additional method for tracking the two-phase interface. These methods include the level set method [19–22], the volume of liquid (VOF) method [23,24], or the combined VOSET method [25,26]. A common problem with these methods is that they do not allow modeling of the nucleation process, which should be considered at the micro or nano scale. This process is crucial for modeling the life cycle of vapor bubbles, in particular, the stage of waiting for the appearance of nuclei, the temperature of the onset of boiling, and the density of nucleation sites. Without the ability to model these characteristics, it is impossible to calculate the boiling curves for an ensemble of bubbles that form on extended surfaces. To simulate micro-nanoscale phenomena, such as the process of nucleation, the molecular dynamics method is well applicable [27–29]. However, its application on a macro scale is difficult due to usually limited computational power.

Lattice Boltzmann Method (LBM) implies a different approach to multiphase flows simulation. In this method, the medium is represented in the form of ensembles of pseudoparticles, for which the kinetic equation is solved in the discrete formulation. Only a small set of pseudoparticle velocities is possible, such that the velocities are directed towards neighboring nodes of the spatial lattice. This method belongs to the mesoscopic category, and occupies an intermediate position between the microscopic method of molecular dynamics and the macroscopic CFD approaches. Despite the complexity of the Boltzmann kinetic equation in the classical formulation, its discrete counterpart is simple and ideally suited for parallel computing. Over 30 years of LBM development, it has proven itself well for modeling both single-phase and multi-phase flows [30,31]. In [32], the LBM with a pseudopotential was presented, in which the interaction function between pseudoparticles is specified. With this approach, phase separation is obtained in a natural way as a consequence of the forces of interaction of pseudoparticles at the lattice sites. The action of body

forces can be specified in different ways, of which the Guo method [33], He method [34] and the exact difference method (EDM) [35] are the most effective. Another important advantage of LBM is the way of specifying the condition at the fluid-solid boundary, the so-called bounce-back condition [36]. This makes it possible to simply set a solid boundary of an arbitrary shape [36], as well as to set an arbitrary local value of the wetting angle [37].

The advantages stated above made it possible to use LBM to model and study the pool boiling processes. Using this method, it is possible to simulate the process of vapor phase nucleation without the need to specify additional initial conditions obtained empirically. The authors of [38,39] used LBM to simulate the processes of growth and detachment of single bubbles during boiling. The dependence of the departure diameter and the frequency of bubble departure on the wetting contact angle and the Jacob number was studied. In [40–44], boiling curves were calculated for smooth surfaces with different uniform wettability. It was shown that the boiling crisis for a lyophobic heater occurs at lower superheats than for a lyophilic one, and an increase in the wetting contact angle leads to a decrease in the CHF. Recently, works have been presented on the LBM simulation of heat transfer processes during boiling on surfaces with contrast wettability [45,46]. The papers simulated boiling on a lyophilic surface with the inclusion of lyophobic zones. The authors demonstrated the possibility of increasing the heat flux compared to a homogeneous lyophilic surface.

The purpose of the paper is to develop a hybrid model based on LBM and heat transfer equations capable of simulating the process of boiling on surfaces with contrast wettability in a wide range of surface superheats up to the boiling crisis development. The model will permit obtaining the boiling curves for heat exchange surfaces with homogeneous and heterogeneous wettability, to study the effect of the size of lyophobic zones on a lyophilic base surface and of the distance between them, and to determine the optimal biphilic surface configuration for efficient heat transfer.

2. Model

For the study of pool boiling processes, a hybrid model based on the standard pseudopotential multiphase Lattice Boltzmann method coupled with the heat transfer equation is used. Below a brief overview of the model is presented while a more detailed description can be found in [39,41]. The basic equation for the time evolution of the density distribution function f_i in a discrete form can be presented in the form:

$$f_i(\vec{x} + \vec{c}_i\Delta t, t + \Delta t) = f_i(\vec{x}, t) + \Omega_i(\vec{x}, t) + S_i(\vec{x}, t), \quad (1)$$

where $\vec{x}$ is the position and t is the dimensionless time, $\vec{c}_i$ are the unit lattice vectors, Ω_i is the collision operator, which describes the particles' interaction, and S_i is the change of the distribution function due to the action of the bulk forces. In the paper, a two dimensional D2Q9 lattice with nine directions is used: $|\vec{c}_i| = (0, 1, \sqrt{2})$, $i = \{1, 2, \ldots, 5, 6, \ldots, 9\}$. The density ρ and the velocity $\vec{u}$ of the medium in each point can be obtained from the moments of the distribution function:

$$\rho(\vec{x}, t) = \sum_i f_i(\vec{x}, t),\ \rho\vec{u}(\vec{x}, t) = \sum_i \vec{c}_i f_i(\vec{x}, t). \quad (2)$$

The Bhatnagar–Gross–Krook (BGK) approximation for a collision operator is used:

$$\Omega_i(\vec{x}, t) = -\frac{f_i - f_i^{eq}}{\tau}. \quad (3)$$

where f_i^{eq} is the equilibrium distribution function, τ is the relaxation time connected with the kinematic viscosity ν as $\tau = 0.5 - \nu/c_s^2$, and where ${c_s}^2 = (1/3)\Delta x^2/\Delta t^2$ is the lattice speed of sound; Δx and Δt are the spatial and time steps.

For the body force term, the exact difference method [35] is used:

$$S_i = f_i^{eq}(\rho, \vec{u} + \Delta\vec{u}) - f_i^{eq}(\rho, \vec{u}) \quad (4)$$

where the change of velocity $\vec{u}$ is determined by the force acting on the node: $\Delta\vec{u} = \vec{F}/\rho$. The total force $\vec{F}$ acting on the particles consists of the following components:

$$\vec{F}(\vec{x}) = \vec{F}_{\text{int}}(\vec{x}) + \vec{F}_s(\vec{x}) + \vec{F}_g(\vec{x}), \quad (5)$$

where $\vec{F}_{\text{int}}(\vec{x})$ is the particles' interaction force responsible for phase separation, $\vec{F}_s(\vec{x})$ describes the interaction of the medium with the solid surface, and $\vec{F}_g(\vec{x}) = g(\rho - \rho_{avg})$ is the gravity force, where ρ_{avg} is the average density of the liquid/vapor medium; g is free fall acceleration.

The equation of state (EOS) of the simulated fluid is defined by $\vec{F}_{\text{int}}(\vec{x})$ written as a gradient of a pseudopotential Ψ as proposed in [32]. The gradient of the pseudopotential is approximated with the finite-difference scheme [35]. In the paper, the Peng–Robinson equation of state [47] is used to determine the pressure dependence $P(\rho,T)$ on the density ρ and the temperature T of the liquid/vapor medium.

In the absence of the fluid-solid interaction (adhesive force), a liquid-solid contact angle θ is equal to 90°. To adjust the value of the contact angle, an approach proposed in [37] is used, and an extra force $\vec{F}_s(\vec{x})$ is added to the nodes near the solid boundary. The contact angle is modeled by varying the strength and direction of the force $\vec{F}_s(\vec{x})$ as described in detail in [37,41]. In the present paper, the contact angles θ = 38°, 90° and 116° are used for the simulation of the lyophilic, neutral and lyophobic surfaces.

Evolution of the heat transfer in the computational region is described by the heat conduction equation taking into account diffusion, convection, work of pressure forces, as well as phase transition [41,42]. In the model, the dimensionless parameters in the lattice units are used. The values of pressure P, temperature T and density ρ are expressed in units P_c, T_c and ρ_c, which correspond to the parameters of the fluid at the critical point. In dimensionless form this equation reads:

$$\frac{\partial T}{\partial t} + \vec{u}_f\vec{\nabla}T = \frac{1}{\rho_c\rho c_v}\vec{\nabla}\left(\lambda\vec{\nabla}T\right)\frac{\Delta t}{\Delta x^2} - \frac{T}{\rho_c\rho c_v}\frac{P_c}{T_c}\left(\frac{\partial p_{EOS}}{\partial T}\right)_\rho \vec{\nabla}\cdot\vec{u}_f, \quad (6)$$

where c_v and λ are the heat capacity and thermal conductivity coefficient. Here, $\vec{u}_f = \vec{u} + \Delta\vec{u}/2$ is the physical velocity of the continuum. The last term in the equation implicitly accounts for the latent heat of vaporization, which is the main source of enhancement of the heat flux under the onset of nucleate boiling.

The computational domain consists of a liquid/vapor medium and a metal heater (see Figure 1). In the paper, 800 spatial cells in a horizontal direction (axis x) and 500 spatial cells in a vertical direction (axis y) are used. The metal heater with a thickness of n_h = 30 spatial cells is placed on the bottom boundary. Spatial and time steps are equal to $\Delta x = 20 \times 10^{-6}$ m and $\Delta t = 2.5 \times 10^{-6}$ s, respectively. Periodic boundary conditions are applied to the left and the right boundaries. On the top boundary, a constant temperature $T_0 = 0.9\ T_c$ and corresponding pressure P_0 are specified. Inside the metal heater, only heat diffusion Equation (6) is solved, with constant temperature T_h condition imposed at the bottom. The calculations were performed for different values of superheat ΔT, i.e., the temperature difference between the top and the bottom boundaries of the solution region, $\Delta T = T_h - T_0$. Thermal conductivity and heat capacity of the metal heater are set to λ_h = 20 W/m/K and $c_h = 3 \times 10^6$ J/m^3, respectively. The thermodynamic properties of the fluid, e.g., heat capacity, thermal conductivity, and viscosity are evaluated based on the current density of the liquid/vapor medium and are parameterized based on the properties of the liquid and its vapor.

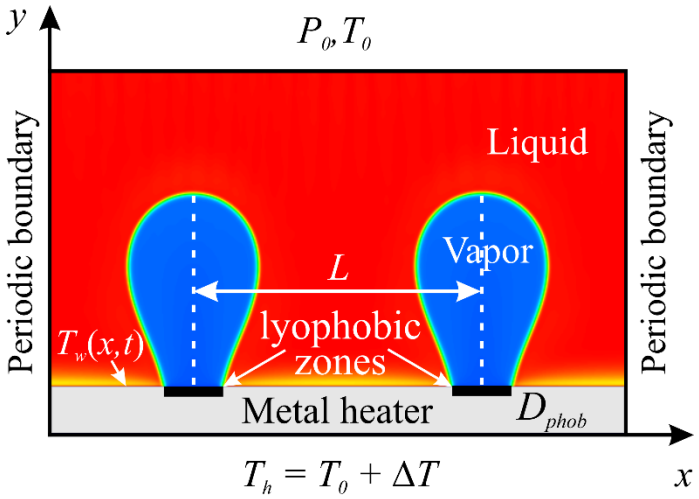


Figure 1. Computational domain and boundary conditions. Layout of the lyophobic zones on the lyophilic surface: D_{phob} is the width of the lyophobic zones, L is the distance between the lyophobic zones.

The phase diagram for some instant at boiling on a biphilic surface is also presented in Figure 1. Areas with the gas phase are shown in blue while the liquid phase is shown in red. The distance between the neighbor lyophobic zones is L and the width of each lyophobic zone is D_{phob}.

3. Results

3.1. Boiling on the Surfaces with Homogenous Wettability

At the initial stage, the boiling curves $<q>(\Delta T')$ were calculated for the smooth surfaces with homogeneous wettability including lyophobic and lyophilic states, where $\Delta T' = <T_w> - T_{sat}$ is the surface superheat and T_{sat} is the saturation temperature (Figure 2). Average heater surface temperature $<T_w>$ is obtained by averaging the temperature $T_w(x,t)$ over time and the heater surface. In calculations, to obtain each point of the dependence $q(\Delta T')$, temperature value is set on the lower wall of the heater T_h = const. The heater surface temperature $T_w(x,t)$ depends on the heat transfer processes and evolves according to the Equation (6), see [41]. In turn, the time and the surface averaged heat flux $<q>$ through the metal heater of the height $H_h = n_h\, h$ is determined as $<q> = -\lambda_h\, (<T_w> - T_h)/H_h$.

As can be seen from the data presented in Figure 2, at low superheats, the boiling curves $q(\Delta T')$ do not depend on the value of the wetting angle, since the heat transfer in this region occurs in the mode of single-phase natural convection. After the onset of boiling, the slope of the $q(\Delta T')$ curves sharply increases, which corresponds to an increase in the intensity of heat transfer with the transition from natural convection to nucleate boiling. It can be seen that the temperature corresponding to ONB (onset of nucleate boiling) noticeably decreases with increasing contact angle, which is in qualitative agreement with the results of experimental studies [8–13]. The analysis of the curves in Figure 2 shows that the heat transfer depends in a complex way on the surface superheats and surface wettability. For example, in the region of low surface superheat, the removal heat flux increases with increasing contact angle, which qualitatively agrees with the results of experiments [9–11], in which it was shown that for weakly hydrophobic surfaces (θ = 116–130°) at low input heat fluxes, an enhancement of heat transfer is observed in comparison with hydrophilic samples. However, as calculations show, the situation changes dramatically in the area of high wall superheats. It can be seen that the value of the CHF decreases significantly with an increase in the contact angle, which also qualitatively agrees with the experimental results [11–13]. Moreover, the boiling crisis on the lyophobic surface can be observed even before the onset of nucleate boiling on the lyophilic surface at a given wall superheat.

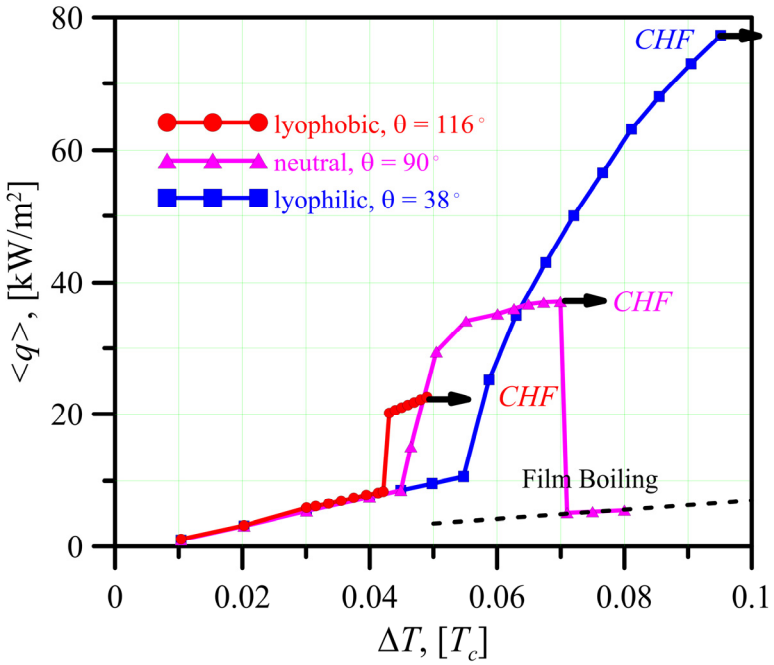


Figure 2. Boiling curves $q(\Delta T')$ for the smooth surfaces with homogeneous wettability: lyophilic surface ($\theta = 38°$), neutral surface ($\theta = 90°$), lyophobic surface ($\theta = 116°$).

Figure 3 shows density contour plots of boiling at low wall superheat ($\Delta T = 0.045\ T_c$) on surfaces with different contact angles. As can be seen from the pictures, at low surface superheats the boiling on homogeneous lyophobic surface ($\theta = 116°$) resembles a transitional boiling regime, when part of the surface is occupied by vapor phase with local sites of film boiling. In general, this picture is similar to the results of experimental studies, in which it was shown that boiling on weakly hydrophobic surfaces in the region of low heat fluxes is characterized by the presence of large-scale sessile bubbles with periodic separation of the vapor phase from liquid-vapor interface [10–12]. It has also been shown in the vast majority of experiments [10–12,48,49] that for lyophobic surfaces, the angle of inclination of the liquid meniscus with respect to the solid body exceeds 90°, and the vapor bubble detaches at some distance from the heater surface. This leads to the fact that after the departure of the vapor bubble, part of the vapor always remains on the surface, which leads to the degeneration of the waiting stage of the appearance of a bubble in the life cycle of the nucleation site. Indeed, the results of LBM simulation on lyophobic surfaces ($\theta \geq 90°$) demonstrate a qualitatively similar behavior of the triple contact line during evolution of vapor bubbles on the heating surface. At the same wall superheat, as can be seen form Figure 3c, the heat transfer on the lyophilic surface ($\theta = 38°$) occurs in the free convection mode without activation of nucleation sites.

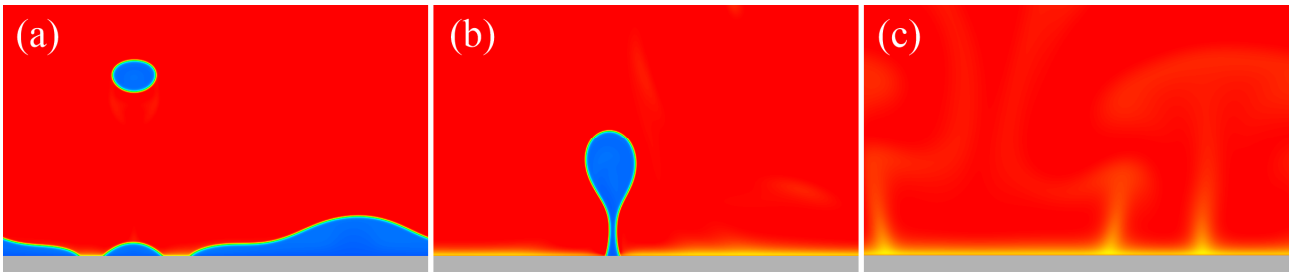


Figure 3. The density contour plots illustrating the boiling process at low surface superheat, $\Delta T = 0.045\ T_c$. (**a**) lyophobic surface ($\theta = 116°$), (**b**) neutral surface ($\theta = 90°$) (**c**) lyophilic surface ($\theta = 38°$).

With an increase in wall superheat $\Delta T = 0.06\ T_c$, the boiling behavior on surfaces with different wettability changes (Figure 4). As can be seen from Figure 4a, in this case for lyophobic surface, the stable film boiling mode is observed, and the entire surface of the heater is covered with a vapor phase with periodic detachment of vapor bubbles from the film surface. For a neutral surface (Figure 4b), with an increase in the input heat flux, several nucleation sites can simultaneously be activated on the surface, which also leads to an increase of vaporization rate compared to the case of low superheat. However, large bubbles with the area bounded by the triple contact line larger than the bubble departure diameter may also appear. For a lyophilic surface at given superheat (Figure 4c), vapor bubbles are already activated in comparison with the case shown in Figure 3c. However, the boiling process seems to have a periodic character, when several nucleation sites are activated at once, and after the detachment of vapor bubbles, a long waiting stage is observed. This leads to noticeable pulsations in the space averaged wall temperature over time. This character of boiling can be related to the fact that an absolutely smooth surface is specified in the simulation model, when there are no cavities which are potential sites for the activation of vapor bubbles. At the same time, the evolution of individual bubbles qualitatively corresponds to experimental observations of the dynamics of growth and detachment of bubbles during boiling of a wide class of liquids on lyophilic surfaces [19–22,38,39].

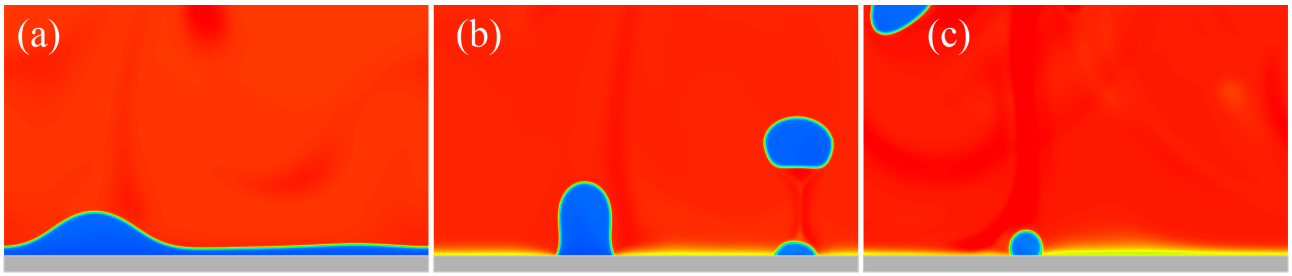


Figure 4. The density contour plots illustrating the boiling process at moderate surface superheat, $\Delta T = 0.06\ T_c$. (**a**) lyophobic surface (θ = 116°), (**b**) neutral surface (θ = 90°) (**c**) lyophilic surface (θ = 38°).

3.2. Bubble Dynamic at Boiling above a Single Lyophobic Zone

In our opinion, the choice of the configuration of the biphilic pattern surface is determined primarily by the selection of the optimal sizes of the lyophobic zones and the distances between them on the lyophilic base. Therefore, at the first stage, the process of vapor bubble growth and detachment for a single lyophobic zone with different sizes (contact angle θ = 116°) located in the center of the smooth lyophilic surface of the heater (θ = 38°) was simulated. In LBM simulation, the following range of widths of the lyophobic zone D_{phob} = 0.3–3 mm was considered, which is noticeably larger than the critical radius of vapor nuclei and smaller or comparable with the bubble departure diameter. Moreover, this range of sizes of the lyophobic zone is, as a rule, used to create biphilic surfaces in experimental works [14–17].

Figure 5 shows the characteristic temporal evolution of a single bubble for a given width of the lyophobic zone D_{phob} = 1.5 mm and a heater temperature $T_h = 0.95\ T_c$. The size of the computational domain was 400 cells horizontally (12 mm) and 600 cells vertically (18 mm). In general, the observed picture of the process is similar to boiling on a lyophobic surface; however, there is some limitation on the size of the contact line region associated with the finite size of the lyophobic spot.

Then, various key characteristics of bubble evolution were studied and dependences of the departure diameter D_d and the departure frequency ν_d of bubbles on the width of the lyophobic zone D_{phob} were plotted (Figure 6). It can be seen that the bubble departure diameter D_d increases almost linearly with the width of the lyophobic zone D_{phob} and changes by 25% in the studied range (Figure 6a). At the same time, on the dependence of the bubble departure frequency ν_d on D_{phob}, shown in Figure 6b, a maximum is observed

at D_{phob} = 450 μm. The higher the bubble departure frequency, the more energy is spent on vaporization averaged over time. The thermal analysis of calculations results also demonstrate that the maximum heat flux removed from the surface is observed also for a lyophobic zone with a width of D_{phob} = 450 μm. Therefore, further we will consider this width of the lyophobic zone as the optimal.

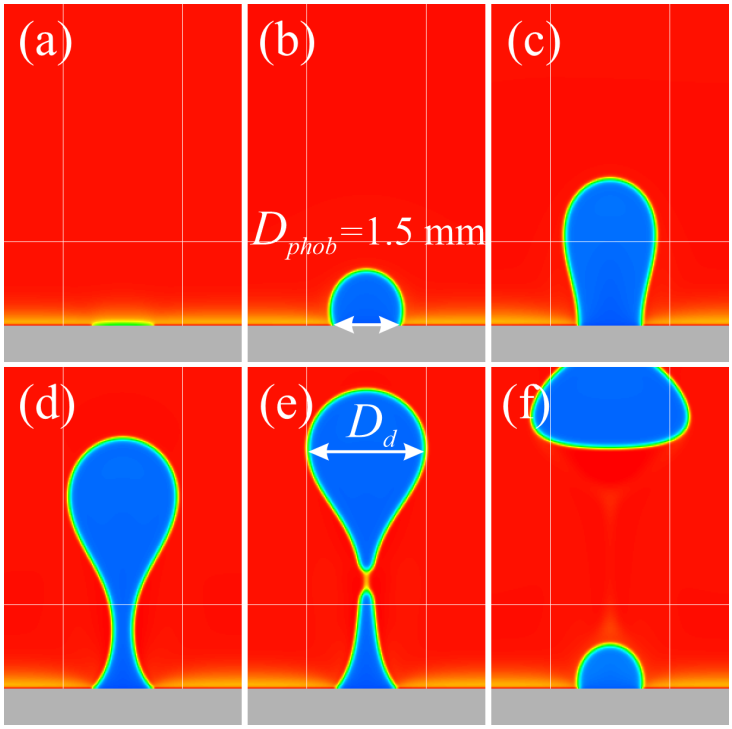


Figure 5. Temporal evolution of the growth and departure of a single bubble: (**a**) t = 0.15 s, (**b**) t = 0.175 s, (**c**) t = 0.375 s, (**d**) t = 0.475 s, (**e**) t = 0.5 s, (**f**) t = 0.525 s. Lyophobic zone size D_{phob} = 1.5 mm, horizontal region size is 12 mm, heater temperature T_h = 0.95 T_c.

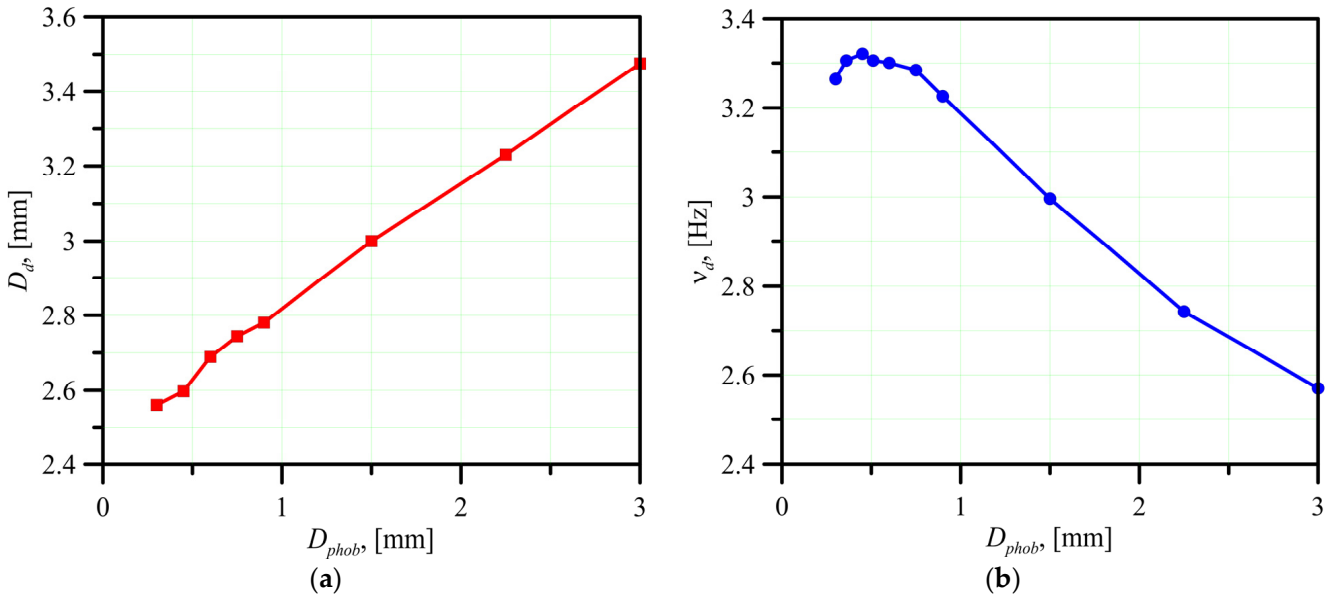


Figure 6. (**a**) Bubble departure diameter D_d and (**b**) departure frequency ν_d depending on the lyophobic zone width D_{phob}. Heater temperature T_h = 0.95 T_c.

3.3. Boiling on the Surfaces with Contrast Wettability

At the next stage, the boiling process was simulated on the surfaces with contrast wettability by changing the distance L between the lyophobic zones (i.e., pitch size) with an optimal spot width D_{phob} = 450 μm. The size of the computational domain was 800 cells horizontally (24 mm) and 500 cells vertically (15 mm). Simulation was carried out for different numbers N = 3, 5, 7, 10, 15 and 20 of lyophobic zones equidistantly located on the lyophilic surface, which corresponded to the range of the distances between the spots L = 1.2–12 mm, and the ratio L/D_d = 0.46–4.61. Thus, such characteristic cases were considered when the distance between the centers of bubble nucleation is less $L/D_d < 1$, corresponds to $L/D_d \sim 1$, and is greater $L/D_d > 1$ than the departure diameter of the bubble. An additional analysis of the density contour plots and temperature fields was carried out in a wide range of input heat flux, which permitted determination of the cause-and-effect relationships between the dependence of the heat transfer efficiency and the boiling behavior for the various configurations of the patterned biphilic surface.

The analysis of boiling curves presented in Figure 7 shows that in the regime of single phase convection ($\Delta T \leq 0.044\ T_c$) the dependencies for surfaces with contrast wettability coincide with the surface with homogeneous wettability. The onset of nucleate boiling on the surfaces with contrast wettability is observed at the same temperature of the heater as on the pure lyophobic surface ($T_{ONB,phob} \approx 0.944\ T_c$), but much lower than on the lyophilic surface ($T_{ONB,phil} \approx 0.955\ T_c$). The calculated curves show that with the development of boiling at $\Delta T > 0.044\ T_c$, the removed heat flux $<q>$ from the biphilic surfaces increases significantly compared to surfaces with homogeneous wettability at a given wall superheat. Calculations also show that at certain surface superheats ($\Delta T \approx 0.07\ T_c$), the intensity of heat transfer on biphilic surfaces begins to decrease in relation to boiling heat transfer on lyophilic surface. It is also seen that at high surface superheat $\Delta T > 0.07\ T_c$, the removed heat flux $<q>$ from the surfaces with contrast wettability decreases with a decrease of the distance L between the lyophobic zones that corresponds to larger number of the zones. It should be noted that the CHF on the surfaces with contrast wettability is lower than the CHF on the lyophilic surface, and the value of the CHF decreases with a decrease of the distance between the lyophobic zones.

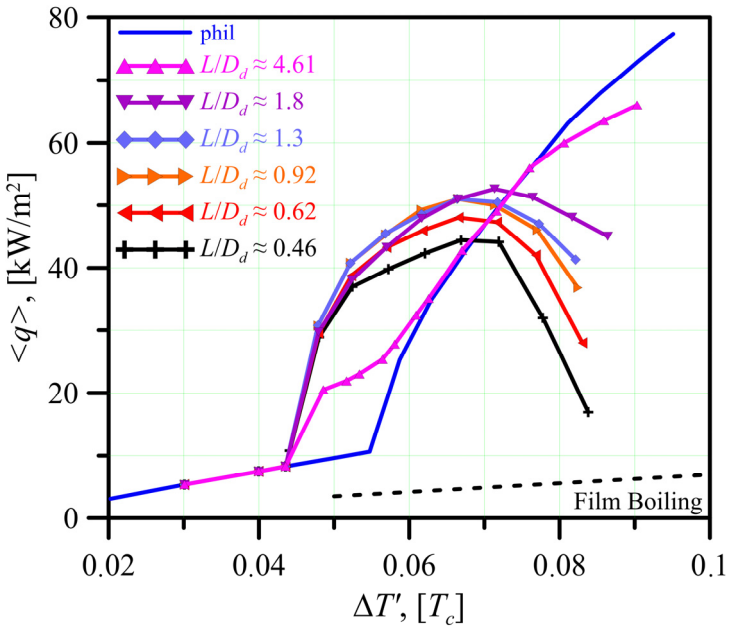


Figure 7. Boiling curves $q(\Delta T')$ for the smooth surfaces with contrast wettability. Lyophobic zone width D_{phob} = 450 μm, space separation between the zones L/D_d = 0.46, 0.62, 0.92, 1.3, 1.8 and 4.61.

Figure 8 shows the density contour plots of boiling on surfaces with contrast wettability for various numbers of lyophobic zones on the lyophilic substrate, N = 2, 7 and 20, at moderate surface superheat $\Delta T = 0.065\ T_c$. On a surface with N = 2 lyophobic zones, the formation of bubbles occurs mainly above these zones, and after the bubble departure, the vapor phase always remains above them. The bubble base then may extend beyond the boundaries of the lyophobic zone due to the small width of the zone itself. The distance between the zones for N = 2 exceeds the separation diameter of the bubble by several times, L/D_d = 4.61, and therefore the bubbles do not interact with each other. For a surface with N = 7 lyophobic zones, the distance between lyophobic zones becomes comparable to the bubble departure diameter, L/D_d = 1.3. Neighbor bubbles begin to interact with each other. As a result of the merging of two adjacent vapor bubbles, some part of the heating surface can be covered by a vapor phase. The usage of the surface with large number of lyophobic zones, N = 20, and, accordingly, a small distance between the spots, L/D_d = 0.62, leads to coalescence of bubbles from neighboring lyophobic zones in the early stages of their evolution, which ultimately leads to an increase in the area occupied by dry spots and a decrease in the intensity of heat transfer during boiling compared to other configurations of biphilic surfaces described above. Figure 7 shows that at moderate surface superheat $\Delta T = 0.065\ T_c$, the heat flux removed from the surface with large distance between the lyophobic zones, L/D_d = 4.61, is much lower than from the surfaces with L/D_d = 1.3 and L/D_d = 0.62. However, the heat flux removed from the surface with low distance between the zones L/D_d = 0.62 is less than from a surface with L/D_d = 1.3. At high surface superheat $\Delta T > 0.07\ T_c$, a significant part of the heating surface is covered by a vapor film due to merging of several bubbles. These local areas of film boiling are quite stable over time, which leads to a noticeable decrease in the intensity of heat transfer for biphilic surfaces with $L/D_d < 1.8$.

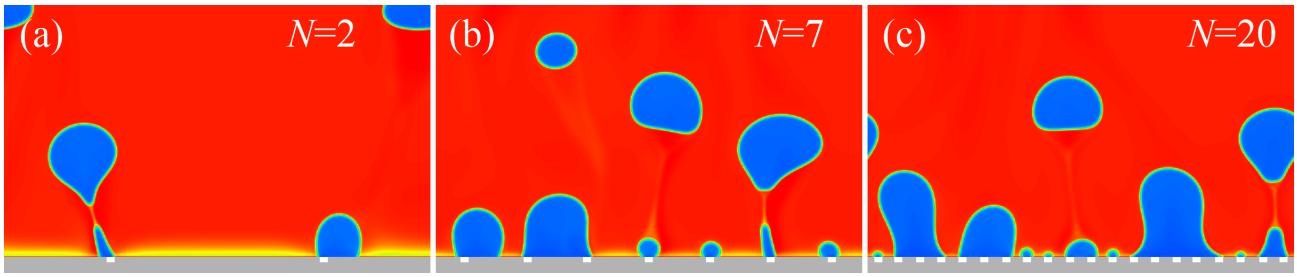


Figure 8. The density contour plots of boiling at $\Delta T = 0.065\ T_c$ for different numbers of the lyophobic zones: (**a**) N = 2 ($L/D_d \approx 4.61$), (**b**) N = 7 ($L/D_d \approx 1.3$), (**c**) N = 20 ($L/D_d \approx 0.62$).

It should be noted that the degradation of heat transfer on modified surfaces with contrast properties compared to the unmodified lyophilic surface was also observed experimentally. In [50], degradation of the heat transfer has been observed with increasing the size of hydrophobic spots. In [51], the formation of a "gigantic single bubble" on the pattered surface was observed as a result of bubbles merging at high surface superheats. A similar effect of heat transfer degradation was observed on a structured surface at a small distance between cavities [52].

3.4. Discussion

Finally, we tried to generalize the obtained results on the enhancement of heat transfer at pool boiling on surfaces with contrast and homogeneous wettability. Let us consider the ratio of the heat transfer coefficient on a biphilic surface to the heat transfer coefficient on a lyophilic surface, HTC/HTC_{phil}. Figure 9 shows the dependences of enhancement factor HTC/HTC_{phil} on the distance between the lyophobic zones for various values of the heater temperature T_h. It can be seen that for moderate heater temperatures, $T_h < 0.96\ T_c$, the enhancement factor on surfaces with contrast wettability is greater than unity. However, at high heater temperatures, $T_h > 0.97\ T_c$, the enhancement factor on the modified surfaces de-

creases due to the presence of wide unwetted areas. It was also found that the dependences of the enhancement factor on the distance between zones L/D_d have a maximum around $L/D_d \sim 1.1$. The maximum values of the enhancement factor $HTC/HTC_{phil} \approx 4$ at heater temperature $T_h = 0.955\ T_c$ were obtained for surfaces with parameters $L/D_d \approx 0.92$ and 1.3. Thus, as a result of the performed numerical simulations, it can be concluded that for moderate surface superheat the optimal distance between the lyophobic zones should be of the order of the bubble departure diameter, $0.9 \leq L/D_d \leq 1.3$ and the ratio of the width of the lyophobic zone to the bubble departure diameter should be of the order of $D_{phob}/D_d \sim 0.16$. Such distance between the lyophobic zones relative to the bubble departure diameter is consistent with the results of experiments [53], in which heat transfer and bubble dynamics were simultaneously analyzed on biphilic surfaces with different configurations.

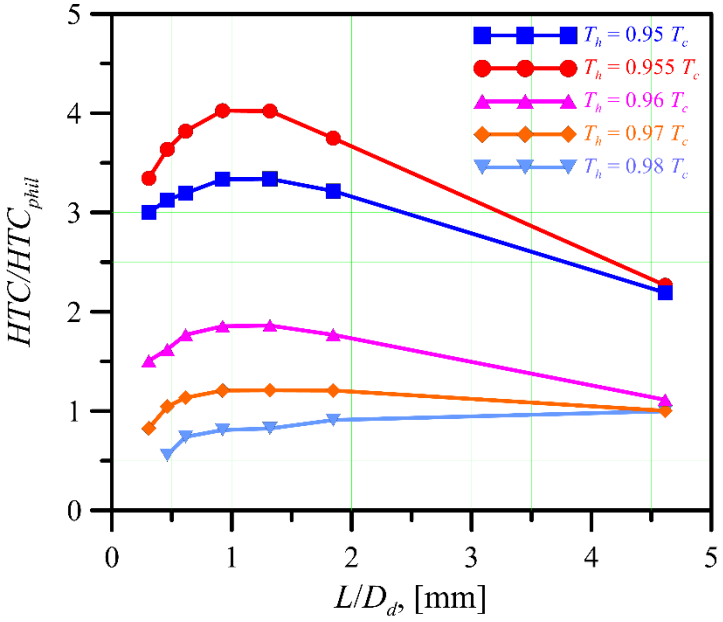


Figure 9. Enhancement factor for heat transfer on the surfaces with contrast wettability depending on the distance between the lyophobic zones L/D_d for different heater temperatures T_h.

It should be emphasized that the simulation results obtained in the paper with the help of hybrid LBM model for the boiling on ideally smooth surfaces do not take into account a number of important aspects related to real experimental situations. First of all, the roughness of heat exchange surfaces leads to some stabilization of the bubbles and influences the nucleation process. Although the liquid parameters given in the model are taken as close as possible to water physical properties, the obtained results correspond to some kind of a model fluid. In the future, it is necessary to carry out simulations varying the properties of the fluid in order to search for universal regularities. It should be also noted that in the model a low liquid to vapor densities ratio ($\rho_l/\rho_v \sim 25$) is considered, that corresponds to the case close to the critical point. Furthermore, 3D modeling could lead to a better agreement with available experimental data than obtained in this work with 2D simulations. Nevertheless, the presented results qualitatively describe the main characteristics of the boiling process, and the abovementioned shortcomings set a task for improvement of the model in the future.

4. Conclusions

In this study, to simulate the pool boiling on smooth surfaces with contrast wettability, a hybrid model based on the lattice Boltzmann method and the heat transfer equation in a two-phase medium was used. As a result of numerical simulation, boiling curves were calculated for surfaces with uniform wettability (lyophilic, neutral and lyophobic surfaces). The process of boiling over a single lyophobic zone on a lyophilic surface was studied, and

dependences of the bubble departure frequency and bubble departure diameter on the width of the spot were obtained that permit calculation of its optimal size. The pool boiling on the surfaces with different configuration of the patterns was studied and the boiling curves were calculated.

The following conclusions were drawn:

- The calculations showed that the use of the surfaces with contrast wettability permits a substantial decrease in the onset of nucleate boiling compared to a bare lyophilic surface. The ONB of biphilic surfaces occurs approximately at the same superheats as on a homogeneous lyophobic surface.
- Based on the simulations of a bubble dynamic at boiling above a single lyophobic zone and on analysis of key characteristics of bubble evolution, i.e., the bubble departure diameter D_d and the bubble departure frequency ν_d, the optimal width of the lyophobic spot $D_{phob}/D_d \sim 0.16$ was obtained.
- It was shown that at moderate surface superheat, the heat transfer at boiling on surfaces with contrast wettability is significantly higher than the heat transfer on the surfaces with uniform wettability.
- In terms of heat transfer performance, the optimal configuration of the biphilic surface at moderate surface superheats was determined: the ratio of the width of the lyophobic zone $D_{phob}/D_d \sim 0.16$ and the distance between the lyophobic zones $0.9 \leq L/D_d \leq 1.3$ to the bubble departure diameter permits enhancement of the heat transfer by more than 4 times. The presented comprehensive studies made it possible to better understand the physics of the boiling process on surfaces with contrast wettability, and to identify the mechanisms of heat transfer enhancement/degradation. Based on the obtained simulation results, an optimal configuration of lyophobic zones on a lyophilic heating surface is proposed for a significant enhancement of boiling heat transfer. This information can already be used for future experiments to simplify the search for optimal configurations of biphilic surfaces for enhancement of boiling heat transfer. At the same time, it is necessary to further improve the numerical model, which would allow not only to control the surface wetting properties, but also to set morphological parameters, as well as to vary the properties of the liquid to simulate real coolants, heat exchange devices and thermal stabilization systems operating in various boiling conditions.

Author Contributions: Conceptualization, A.V.F. and A.S.S.; methodology, A.V.F. and A.E.O.; formal analysis, A.V.F. and A.S.S.; writing—original draft preparation, A.V.F., M.V.S., A.E.O. and A.S.S.; writing—review and editing, A.V.F., M.V.S., A.E.O. and A.S.S. All authors have read and agreed to the published version of the manuscript.

Funding: This research was funded by Russian Science Foundation grant number 22-29-01251.

Data Availability Statement: Data are available from the authors.

Conflicts of Interest: The authors declare no conflict of interest.

References

1. Liang, G.; Mudawar, I. Review of pool boiling enhancement by surface modification. *Int. J. Heat Mass Transf.* **2019**, *128*, 892–933. [CrossRef]
2. Sajjad, U.; Sadeghianjahromi, A.; Muhammad, H.A.; Wang, C.C. Enhanced pool boiling of dielectric and highly wetting liquids—A review on enhancement mechanisms. *Int. J. Heat Mass Transf.* **2020**, *119*, 104950. [CrossRef]
3. Mehralizadeh, A.; Shabanian, S.; Bakeri, G. Effect of modified surfaces on bubble dynamics and pool boiling heat transfer enhancement: A review. *Therm. Sci. Eng. Prog.* **2019**, *15*, 100451. [CrossRef]
4. Khan, S.A.; Atieh, M.A.; Koç, M. Micro-nano scale surface coating for nucleate boiling heat transfer: A critical review. *Energies* **2018**, *11*, 3189. [CrossRef]
5. Surtaev, A.; Serdyukov, V.; Pavlenko, A. Nanotechnologies for thermophysics: Heat transfer and crisis phenomena at boiling. *Nanotech. Russ.* **2016**, *11*, 696–715. [CrossRef]
6. Rahman, M.; Olceroglu, E.; McCarthy, M. Role of wickability on the critical heat flux of structured superhydrophilic surfaces. *Langmuir* **2014**, *30*, 11225–11234. [CrossRef]

7. Xie, S.; Beni, M.S.; Cal, J.; Zhao, J. Review of critical-heat-flux enhancement methods. *Int. J. Heat Mass Transf.* **2018**, *122*, 275–289. [CrossRef]
8. Bourdon, B.; Rioboo, R.; Marengo, M.; Gosselin, E.; De Coninck, J. Influence of the wettability on the boiling onset. *Langmuir* **2012**, *28*, 1618–1624. [CrossRef]
9. Betz, A.; Jenkins, J.; Kim, C.; Attinger, D. Boiling heat transfer on superhydrophilic, superhydrophobic, and superbiphilic surfaces. *Int. J. Heat Mass Transf.* **2013**, *57*, 733–741. [CrossRef]
10. Safonov, A.I.; Kuznetsov, D.V.; Surtaev, A.S. Fabrication of Hydrophobic Coated Tubes for Boiling Heat Transfer Enhancement. *Heat Transf. Eng.* **2020**, *42*, 1390–1403. [CrossRef]
11. Surtaev, A.; Koşar, A.; Serdyukov, V.; Malakhov, I. Boiling at subatmospheric pressures on hydrophobic surface: Bubble dynamics and heat transfer. *Int. J. Therm. Sci.* **2022**, *173*, 107423. [CrossRef]
12. Teodori, E.; Valente, T.; Malavasi, I.; Moita, A.S.; Marengo, M.; Moreira, A.L.N. Effect of extreme wetting scenarios on pool boiling conditions. *Appl. Therm. Eng.* **2017**, *115*, 1424–1437.
13. Phan, H.; Caney, N.; Marty, P.; Colasson, S.; Gavillet, J. Surface wettability control by nanocoating: The effects on pool boiling heat transfer and nucleation mechanism. *Int. J. Heat Mass Transf.* **2009**, *52*, 5459–5471. [CrossRef]
14. Motezakker, A.; Sadaghiani, A.K.; Çelik, S.; Larsen, T.; Villanueva, L.G.; Kosar, A. Optimum ratio of hydrophobic to hydrophilic areas of biphilic surfaces in thermal fluid systems involving boiling. *Int. J. Heat Mass Transf.* **2019**, *135*, 164–174.
15. Može, M.; Zupančič, M.; Golobič, I. Pattern geometry optimization on superbiphilic aluminum surfaces for enhanced pool boiling heat transfer. *Int. J. Heat Mass Transf.* **2020**, *161*, 120265.
16. Cheng, H.C.; Jiang, Z.X.; Chang, P.H.; Chen, P.H. Effects of difference in wettability level of biphilic patterns on copper tubes in pool boiling heat transfer. *Exp. Therm. Fluid Sc.* **2021**, *120*, 110241.
17. Serdyukov, V.; Patrin, G.; Malakhov, I.; Surtaev, A. Biphilic surface to improve and stabilize pool boiling in vacuum. *Appl. Therm. Eng.* **2022**, *209*, 118298.
18. Kharangate, C.R.; Mudawar, I. Review of computational studies on boiling and condensation. *Int. J. Heat Mass Transf.* **2017**, *108*, 1164–1196. [CrossRef]
19. Son, G.; Dhir, V.K.; Ramanujapu, N. Dynamics and Heat Transfer Associated With a Single Bubble during Nucleate Boiling on a Horizontal Surface. *ASME J. Heat Transf.* **1999**, *121*, 623–632.
20. Mukherjee, A.; Dhir, V.K. Study of lateral merger of vapor bubbles during nucleate pool boiling. *J. Heat Transf.* **2004**, *126*, 1023–1039.
21. Mukherjee, A.; Kandlikar, S.G. Numerical study of single bubbles with dynamic contact angle during nucleate pool boiling. *Int. J. Heat Mass Transf.* **2007**, *50*, 127.
22. Duan, X.; Phillips, B.; McKrell, T.; Buongiorno, J. Synchronized High-Speed Video, Infrared Thermometry, and Particle Image Velocimetry Data for Validation of Interface-Tracking Simulations of Nucleate Boiling Phenomena. *Exp. Heat Transf.* **2013**, *26*, 169–197.
23. Kunkelmann, C.; Stephan, P. CFD simulation of boiling flows using the volume of fluid method within OpenFOAM. *Numer. Heat Transf. A Appl.* **2009**, *56*, 631–646. [CrossRef]
24. Jiaqiang, E.; Zhang, Z.; Tu, Z.; Zuo, W.; Hu, W.; Han, D.; Jin, Y. Effect analysis on flow and boiling heat transfer performance of cooling water-jacket of bearing in the gasoline engine turbocharger. *Appl. Therm. Eng.* **2018**, *130*, 754–766.
25. Sun, D.L.; Tao, W.Q. A coupled volume-of-fluid and level set (VOSET) method for computing incompressible two-phase flows. *Int. J. Heat Mass Transf.* **2010**, *53*, 645–655. [CrossRef]
26. Ling, K.; Li, Z.Y.; Tao, W.Q. A direct numerical simulation for nucleate boiling by the VOSET method. *Numer. Heat Transf. A Appl.* **2014**, *65*, 949–971. [CrossRef]
27. She, X.; Shedd, T.A.; Lindeman, B.; Yin, Y.; Zhang, X. Bubble formation on solid surface with a cavity based on molecular dynamics simulation. *Int. J. Heat Mass Transf.* **2016**, *95*, 278–287.
28. Chen, Y.; Zou, Y.; Sun, D.; Wang, Y.; Yu, B. Molecular dynamics simulation of bubble nucleation on nanostructure surface. *Int. J. Heat Mass Transf.* **2018**, *118*, 1143–1151.
29. Zhang, L.; Xu, J.; Liu, G.; Lei, J. Nucleate boiling on nanostructured surfaces using molecular dynamics simulations. *Int. J. Therm. Sci.* **2020**, *152*, 106325.
30. Succi, S. *The Lattice Boltzmann Equation for Fluid Dynamics and Beyond*; Oxford University Press: Oxford, MI, USA, 2001; p. 304.
31. Chen, S.; Doolen, G.D. Lattice Boltzmann method for fluid flows. *Ann. Rev. Fluid Mech.* **1998**, *30*, 329–364.
32. Shan, X.; Chen, H. Lattice Boltzmann model for simulating flows with multiple phases and components. *Phys. Rev. E* **1993**, *47*, 1815–1820. [CrossRef] [PubMed]
33. Guo, Z.; Zheng, C.; Shi, B. Discrete lattice effects on the forcing term in the lattice Boltzmann method. *Phys. Rev. E* **2002**, *65*, 46308. [CrossRef] [PubMed]
34. He, X.; Shan, X.; Doolen, G. Discrete Boltzmann equation model for nonideal gases. *Phys. Rev. E Rapid Comm.* **1998**, *57*, 13. [CrossRef]
35. Kupershtokh, A.L. Incorporating a body force term into the lattice Boltzmann equation. *Vestnik NGU Quart. J. Novosibirsk State Univ. Ser. Math. Mech. Inform.* **2004**, *4*, 75–96.
36. Chen, S.; Martínez, D. On boundary conditions in lattice Boltzmann methods. *Phys. Fluid.* **1996**, *8*, 2527–2536. [CrossRef]

37. Li, Q.; Luo, K.H.; Kang, Q.J.; Chen, Q. Contact angles in the pseudopotential lattice Boltzmann modeling of wetting. *Phys. Rev. E* **2014**, *90*, 053301.
38. Gong, S.; Cheng, P. Lattice Boltzmann simulation of periodic bubble nucleation, growth and departure from a heated surface in pool boiling. *IJHMT* **2013**, *64*, 122–132. [CrossRef]
39. Fedoseev, A.V.; Surtaev, A.S.; Moiseev, M.I.; Ostapchenko, A.E. Lattice Boltzmann simulation of bubble evolution at boiling on surfaces with different wettability. *J. Phys. Conf. Ser.* **2020**, *1677*, 012085.
40. Gong, S.; Cheng, P. Lattice Boltzmann simulations for surface wettability effects in saturated pool boiling heat transfer. *Int. J. Heat Mass Transf.* **2015**, *85*, 635–646. [CrossRef]
41. Moiseev, M.I.; Fedoseev, A.; Shugaev, M.V.; Surtaev, A.S. Hybrid thermal lattice Boltzmann model for boiling heat transfer on surfaces with different wettability. *Int. Phenom. Heat Transf.* **2020**, *8*, 81. [CrossRef]
42. Li, Q.; Kang, Q.J.; Francois, M.M.; He, Y.L.; Luo, K.H. Lattice Boltzmann modeling of boiling heat transfer: The boiling curve and the effects of wettability. *Int. J. Heat Mass Transf.* **2015**, *85*, 787–796. [CrossRef]
43. Fang, W.Z.; Chen, L.; Kang, Q.J.; Tao, W.Q. Lattice Boltzmann modeling of pool boiling with large liquid-gas density ratio. *Int. J. Therm. Sci.* **2017**, *114*, 172–183. [CrossRef]
44. Zhang, C.; Cheng, P. Mesoscale simulations of boiling curves and boiling hysteresis under constant wall temperature and constant heat flux conditions. *Int. J. Heat Mass Transf.* **2017**, *110*, 319. [CrossRef]
45. Gong, S.; Cheng, P. Numerical simulation of pool boiling heat transfer on smooth surfaces with mixed wettability by lattice Boltzmann method. *Int. J. Heat Mass Transf.* **2015**, *80*, 206–216. [CrossRef]
46. Li, Q.; Yu, Y.; Zhou, P.; Yan, H.J. Enhancement of Boiling Heat Transfer Using Hydrophilic-Hydrophobic Mixed Surfaces: A Lattice Boltzmann Study. *Appl. Therm. Eng.* **2018**, *132*, 490–499. [CrossRef]
47. Peng, Y.; Laura, S. Equations of state in a lattice Boltzmann model. *Phys. Fluids* **2006**, *18*, 042101.
48. Nam, Y.; Wu, J.; Warrier, G.; Ju, Y.S. Experimental and numerical study of single bubble dynamics on a hydrophobic surface. *J. Heat Transf.* **2009**, *131*, 121004. [CrossRef]
49. Kim, S.H.; Lee, G.C.; Kang, J.Y.; Moriyama, K.; Park, H.S.; Kim, M.H. The role of surface energy in heterogeneous bubble growth on ideal surface. *Int. J. Heat Mass Transf.* **2017**, *108*, 1901–1909. [CrossRef]
50. Jo, H.; Ahn, H.S.; Kang, S.; Kim, M.H. A study of nucleate boiling heat transfer on hydrophilic, hydrophobic and heterogeneous wetting surfaces. *Int. J. Heat Mass Transf.* **2011**, *54*, 5643. [CrossRef]
51. Choi, C.H.; David, M.; Gao, Z.; Chang, A.; Allen, M.; Wang, H.; Chang, C.H. Large-scale Generation of Patterned Bubble Arrays on Printed Bi-functional Boiling Surfaces. *Sci. Rep.* **2016**, *6*, 23760. [CrossRef]
52. Nimkar, N.D.; Bhavnani, S.H.; Jaeger, R.C. Effect of nucleation site spacing on the pool boiling characteristics of a structured surface. *Int. J. Heat Mass Transf.* **2006**, *49*, 2829. [CrossRef]
53. Lim, D.Y.; Bang, I.C. Controlled bubble departure diameter on biphilic surfaces for enhanced pool boiling heat transfer performance. *Int. J. Heat Mass Transf.* **2020**, *150*, 119360. [CrossRef]